Available online at www.sciencedirect.com
ScienceDirect
C. R. Physique 10 (2009) 305–319
COMPTES RENDUS PHYSIQUE

Carbon nanotube electronics / Électronique à nanotubes de carbone

Multiscale simulation of carbon nanotube devices

C. Adessi [a], R. Avriller [g], X. Blase [b], A. Bournel [c], H. Cazin d'Honincthun [c], P. Dollfus [c], S. Frégonèse [d], S. Galdin-Retailleau [c], A. López-Bezanilla [e], C. Maneux [d], H. Nha Nguyen [c], D. Querlioz [c], S. Roche [e], F. Triozon [f,*], T. Zimmer [d]

[a] *Laboratoire de physique de la matière condensée et des nanostructures, CNRS, université Claude-Bernard Lyon I, UMR 5586, 69622 Villeurbanne cedex, France*
[b] *Institut Néel, CNRS, université Joseph-Fourier, B.P. 166, 38042 Grenoble cedex 09, France*
[c] *Institut d'électronique fondamentale, CNRS, université Paris-Sud (UMR 8622), 91405 Orsay cedex, France*
[d] *IMS, université Bordeaux 1, CNRS, UMR 5218, 33405 Talence, France*
[e] *Commissariat à l'énergie atomique, INAC, SP2M, L_Sim, 17, rue des Martyrs, 38054 Grenoble cedex, France*
[f] *Commissariat à l'énergie atomique, Leti-MINATEC, 17, rue des Martyrs, 38054 Grenoble cedex, France*
[g] *Departamento de Física Teórica de la Materia Condensada c-v, Facultad de Ciencias, Universidad Autónoma de Madrid, E-28049 Madrid, Spain*

Abstract

In recent years, the understanding and accurate simulation of carbon nanotube-based devices has become very challenging. Conventional simulation tools of microelectronics are necessary to envision the performance and use of nanotube transistors and circuits, but the models need to be refined to properly describe the full complexity of such novel type of devices at the nanoscale. Indeed, many issues such as contact resistance, low dimensional electrostatics and screening effects, as well as nanotube doping or functionalization, demand for more accurate quantum approaches. In this article, we review our recent progress on multiscale simulations which aim at bridging first principles calculations with compact modelling, including the comparison between semi-classical Monte Carlo and quantum transport approaches. ***To cite this article: C. Adessi et al., C. R. Physique 10 (2009).***

Résumé

Simulation multi-echelle des dispositifs à nanotube de carbone. Ces dernières années, la compréhension et la simulation précise des dispositifs à base de nanotubes de carbone est devenue une tâche ambitieuse. Les outils de simulation conventionnels de la microélectronique sont nécessaires pour imaginer les performances et l'utilisation des transistors et des circuits à base de nanotubes, mais les modèles doivent être affinés pour décrire correctement la complexité de ces nouveaux types de dispositifs à l'échelle nanométrique. En effet, de nombreuses questions comme la résistance de contact, l'électrostatique en basse dimensionalité et les effets d'écrantage, ainsi que le dopage ou la fonctionnalisation des nanotubes, nécessitent des approches quantiques plus précises. Dans cet article, nous exposons nos progrès récents sur des simulations multi-échelles qui visent à connecter des calculs basés sur les premiers principes à la modélisation compacte, en passant par la comparaison entre l'approche Monte Carlo semi-classique et le transport quantique. ***Pour citer cet article : C. Adessi et al., C. R. Physique 10 (2009).***

Keywords: Carbon nanotubes; Simulation; Electronic transport; Transistors; Circuits; Ab initio calculations

* Corresponding author.
E-mail address: francois.triozon@cea.fr (F. Triozon).

1631-0705/$ – see front matter
doi:10.1016/j.crhy.2009.05.004

Mots-clés : Nanotubes de carbone ; Simulation ; Tranport électronique ; Transistors ; Circuits ; Calculs ab initio

1. Introduction

Carbon nanotubes (CNT) have become key materials to envisage the future of BEYOND-CMOS nanoelectronics [1]. Indeed CNT show unprecedented ballistic transport ability, and large charge mobility, which allow one to fabricate CNT-based field effect transistors (CNTFET) with highly competitive performance [2–5]. Further, CNT are mechanically very stable and can convey very large current density, appearing thus as ideal interconnects in nanosized devices. Finally, due to their specific geometry, novel types of applications have been demonstrated, such as chemical sensing or an optically induced switching mechanism [6]. However, to reach a mature state of CNT technology development, there is a crucial need for advanced simulations of CNT-based devices, since a large dispersion of experimental measurements are usually obtained. This demands for an accurate simulation of nanotube–transistor current–voltage characteristics, and understanding of the role of CNT diameter, metal/nanotube interface, chemical doping, and Schottky Barrier features, which generally monitor device performance. To that aim, a multiscale modelling strategy needs to be developed, from first-principles calculations to compact modelling and circuit simulation. In the following, Section 2 will first present the available compact models for ohmic CNTFETs that already allow one to simulate simple circuits such as oscillators. Section 3 will further describe Monte Carlo transport approaches that are based on a semi-classical description of electronic transport, and which allow the improvement of compact models. Section 4 will present quantum simulations of CNTFETs using either the Wigner Monte Carlo formalism or the non-equilibrium Green's functions (NEGF). In Section 5, first-principle calculations will be presented, together with their bridging to Green's functions transport calculations. This quantum transport framework more easily enables one to account for chemical complexity at the nanoscale, including interface issues, chemical doping, and functionalization. Comparison and complementarities between the different levels of modelling will be discussed.

2. Compact modelling and circuit simulation

To predict the ultimate performance of novel nanodevices such as CNTFETs, and to offer further guidance and cost reduction for technological development, accurate and reliable simulation tools appear as key issues. Among the simulation tools, compact modelling (SPICE-like) is a valuable one to assess the actual potentialities of a given device technology. In this section, several aspects of the evaluation of the CNTFET capability in a circuit context are developed. This evaluation requires an appropriate device model, not only compatible with up-to-date circuit design flows but also computationally efficient and physics-based. The question of the physics-based CNTFET model is addressed in Section 3.2 through dedicated comparisons with Monte Carlo simulation results. We focus here on the compact modelling purpose.

2.1. Five stages ring oscillator

One of the most important challenges of the next decade is to control the technological fluctuations due to size reduction or surface/volume ratio increase. Concerning CNTFET devices, many sources of technological dispersions are to be pointed out like nanotube doping, metal-nanotube contact and nanotube chirality. Many efforts are made to control the nanotube diameter or chirality [7,8], nanotube position and chirality using selected growth [8,9], nanotubes alignment [9] or to pick out the most interesting nanotubes by removing metallic nanotubes and by selecting the chirality [10]. Ring oscillators are often used as a figure of merit to evaluate the performance of a digital technology. Fig. 1 presents the oscillograms of two ring oscillators: case 1 is the result of circuit simulation using the standard compact model parameter set (see Section 2.2 and Fig. 6, except for chirality parameter: $(n, m) = (14, 0)$ since this value correspond to the mean diameter of the dispersion [11]). Case 2 presents results using transistor parameters extracted randomly from technological dispersion [11–13]. From the circuit simulation results, oscillation frequency and power consumption can be extracted for each randomly built circuit. Fig. 1 points out that technological dispersion may have a significant impact on circuit operation: oscillation frequency and power consumption.

To get deeper insight into those circuit figures of merit according to technological dispersion, we have performed an analysis which is summarized in Fig. 1, resulting from 100 randomly-built circuits. Three major dispersion parameters

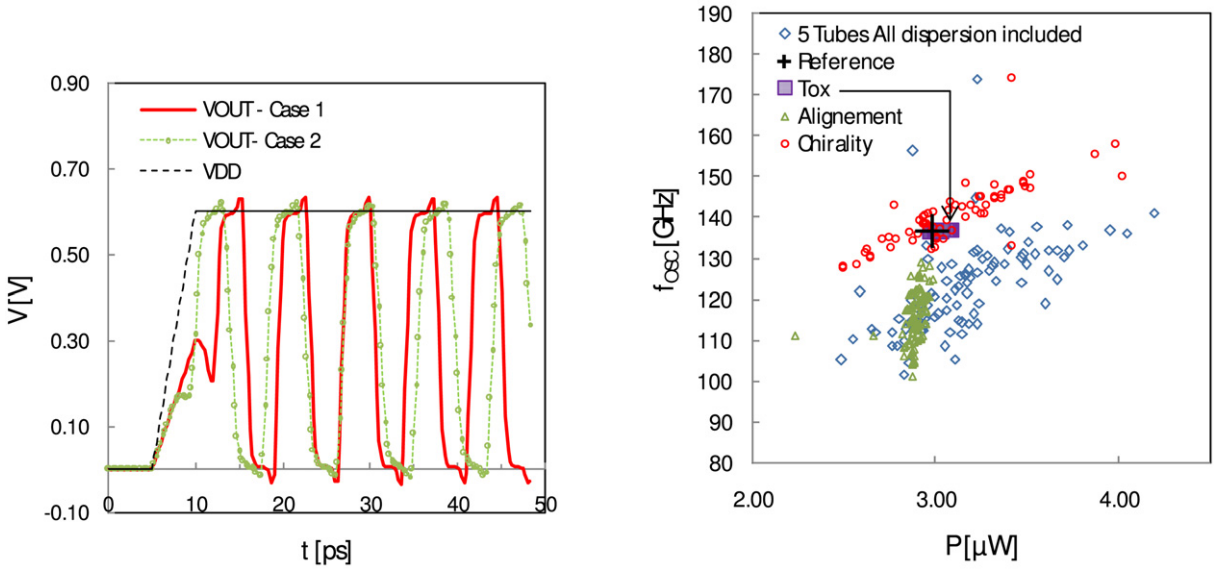

Fig. 1. Left: Oscillograms of the output voltage for two different 5 stages ring oscillator circuits: case 1 uses the reference transistor and case 2 uses random parameters within the range of dispersion. V_{DD} is the circuit bias. Each transistor is made of five tubes without accounting for parasitic elements (fringe capacitance and interconnect capacitance). Right: Scattering plot of oscillation frequency versus power consumption per nanotube ($V_{DD} = 0.6$ V). Simulation of 100 ring oscillator circuits with random parameters extracted from technological dispersion characteristics; transistors are made of five tubes (each tube features different technological parameters); The black cross is the circuit simulated using the reference transistor. Three kinds of technological dispersion are studied independently: gate insulator thickness $T_{OX} = 3$ nm with $\sigma_{TOX} = 0.3$ nm [13], nanotube alignment dispersion (derived from [12]) and nanotube chirality (described in [11]). Finally, the simulation including the whole set of dispersion is presented (diamonds).

have been included in the simulation: nanotube chirality, nanotube misalignment, and gate insulator oxide thickness. Nanotube chirality dispersion [11], gate oxide thickness dispersion [13] and nanotube alignment dispersion [12] are extracted from real fabrication processes. First, each dispersion has been studied independently, and then the whole dispersions have been gathered. The main conclusions are:

– The oxide thickness impact is small compared with other kind of dispersions;
– The nanotube misalignment has a strong impact on oscillation frequency while slightly influencing power consumption. Indeed, since the alignment of the nanotube has an impact on the effective length of the CNTFET channel, the stored charge increases and phonon-carrier scattering mechanisms decrease slightly the ON current;
– The chirality of the tube strongly changes the I_{OFF} current and also changes the I_{ON} current through changes in threshold voltage and gate capacitance. In this case, the power consumption is more affected than the oscillation frequency.

2.2. *CNTFET compact model description*

The results shown above stem from ADS 2004A simulation tool where the structure of the five ring oscillator has been described (Fig. 2). In this software, the CNTFET compact model has been implemented using VerilogA as description language. This program includes large signal equivalent circuit (Fig. 2) and calculates the drain current for given V_{GS} and V_{DS} of an n-type CNTFET including possible serial access resistance. It allows the simulation of a device with SWNT diameter ranging from 0.8–3 nm. To describe the required CNT, two possibilities are open to the designer: choosing the diameter or entering the n and m parameters of the chirality vector. The transistor core is described through the drain current equation I_{DS} derived from the Landauer formula, which describes ballistic transport with ideal ohmic contacts as a function of the channel potential, V_{CNT}. Indeed, as the gate bias voltage V_G increases, the top of the source–channel energy barrier is reduced, which lowers the channel potential V_{CNT} and causes an accumulation of charge Q_{CNT} in the channel [14,15]. This charge Q_{CNT} induces a new voltage drop $V_G - V_{CNT}$

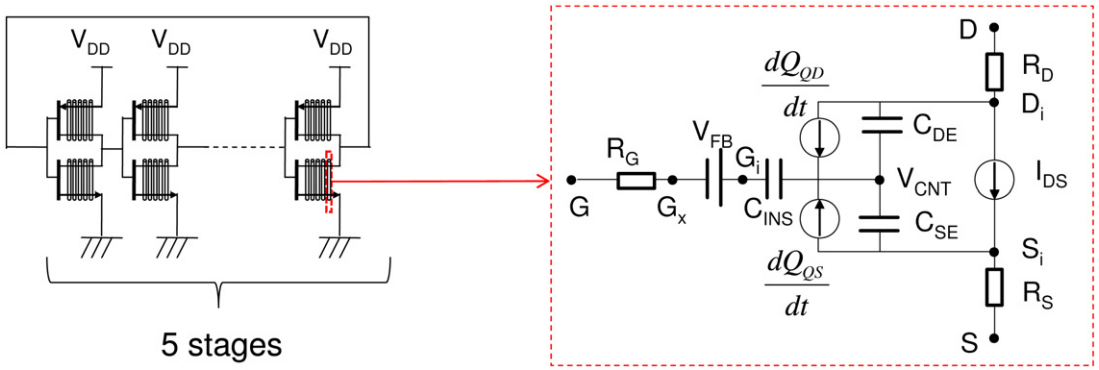

Fig. 2. Equivalent circuits showing the structure of the ring oscillator (left) and the conventional CNTFET model (right).

across the insulator, which causes a modulation of the energy bands. This self-consistent loop in the device operation is handled through an analytical development. The soundness of the whole approach has been evaluated through comparison with the results from CNTFET compact model and from Monte Carlo simulation [16] (see Section 3.2). In particular, this common approach has led one to:

– confirm that all the compact model parameters are physically relevant including the flat band potential, V_{FB};
– define a trade-off between the gate capacitance C_{INS} and the gate bias values that should be used as a design rule for circuit designers.

3. Semi-classical Monte Carlo simulation

The particle-based Monte Carlo (MC) technique is acknowledged as a powerful method for accurately describing carrier transport in semiconductor materials and devices within the semi-classical approximation, i.e. the Boltzmann transport equation (BTE) for the distribution function, including all relevant scattering mechanisms. Extensive overviews of this method may be found in [17,18]. In spite of disadvantages due to large computational requirements and some limitations inherent in the finite number of simulated particles, this technique of transport simulation turns out to be robust, versatile, essentially free from numerical difficulties and thus suitable for device simulation even in three-dimensional (3-D) real space. It may also include quantization effects in field-effect transistors via appropriate coupling with Schrödinger's equation and even quantum transport through the Wigner formalism [19]. The problem of quantum transport will be addressed in the next section. We focus here on the semi-classical case.

3.1. Model and simulation results

The energy dispersion of ideal nanotubes can be obtained from tight-binding calculations including tube curvature effects and the influence of mixing of in-plane σ and out of plane π carbon orbitals. The unit cell of a semiconducting zigzag CNT $(n, 0)$ contains $4n$ atoms with 4 orbitals per atom, which leads to $16n$ valence and conduction subbands. Here we consider the three lowest subbands which are twofold degenerate in two valleys, each of them centred on a graphene K point. In the energy range 0–1.5 eV, the energy dispersion of these subbands can be fitted by analytical approximations [20] conveniently used for the computation of carrier trajectories and scattering rates [21]. We focus on the zigzag CNT $(19, 0)$ with diameter $d_t = 1.5$ nm, subband energies of $0.275, 0.61, 1.06$ eV (measured from the midgap energy) and effective masses of $0.048, 0.129, 0.132$ for the three first subbands, respectively.

The electron phonon scattering rates are calculated using the Fermi golden rule within the deformation potential model. Intra-subband acoustic scattering is treated as an elastic process while inter-subband transitions are considered through the associated finite phonon energy [21]. Finally, the radial breathing phonon mode, which is typical of single-wall carbon nanotubes is also included [22].

For device simulation, the MC transport algorithm is self-consistently coupled with either a 3D Poisson solver based on a finite-element scheme or a 2D Poisson solver considering the cylindrical symmetry of gate-all-around (GAA) devices. In CNTFETs source and drain contacts are either Schottky or ohmic-like. In the latter case, boundary

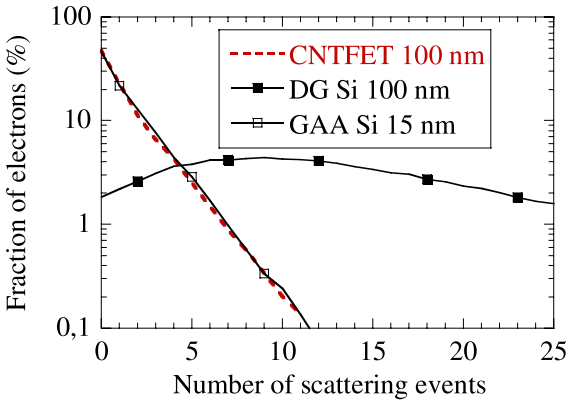

Fig. 3. Fraction of electrons crossing the channel as a function of the number of scattering events ($V_{GS} = V_{DS} = 0.4$ V); comparison with 100 nm-long Double-Gate Si MOSFET (DG Si) and 15 nm-long Gate-All-Around Si MOSFET (GAA Si, 5 nm × 5 nm cross section, $V_{GS} = V_{DS} = 0.7$ V).

conditions are assumed to be characterized by thermal equilibrium and local charge neutrality. After each time step, the appropriate number of electrons is injected at each ohmic contact to recover this neutrality condition. The wave vector coordinates of injected carriers are randomly sampled from a Fermi–Dirac distribution. The possibility of Schottky contact was recently implemented as follows. After each time step the number of injected particles is determined according to the current calculated from the Landauer formula and a transmission coefficient calculated within the WKB approximation [23].

Prior to the presentation of device simulation, it should be mentioned that the transport properties in zigzag semiconducting CNTs were investigated under uniform electric field [21]. It was shown that at low electric field, i.e. smaller than 10 kV/cm, the transport is dominated by low-energy acoustic phonon scattering with mean free path higher than 100 nm and weakly dependent on electric field. At increasing electric field intervalley high-energy phonon scattering becomes dominant, which drastically reduces the mean free path to 20 nm at 100 kV/cm whatever the tube diameter. In a device operating under low electric field the transport is thus likely to have a strong ballistic part.

We first simulated GAA CNTFETs with ohmic contacts on n-doped CNT extensions of 20 nm at the source and drain ends. The nanotube channel is 100 nm long and is surrounded by an insulator layer with dielectric constant $k = 16$ (HfO_2). We considered different equivalent silicon oxide thicknesses (EOT) ranging between 0.17 and 10 nm.

The possibility of quasi-ballistic transport in a CNTFET is well illustrated in Fig. 3 where we plot the fraction of electrons as a function of the number of scattering events experienced in the channel. The result for a 100 nm-long CNTFET is compared with those of a 15 nm-long Si GAA MOSFET and of 100 nm double gate (DG) MOSFET. For the latter, the scattering number distribution is a bell curve and the fraction of ballistic electrons is less than 2%. For a channel length of 100 nm, the CNTFET exhibits a fraction of ballistic electrons of 50% comparable to that of a 15 nm long GAA Si FET. In this case of quasi-ballistic transport the distribution decreases exponentially as a function of the number of scattering events.

In Fig. 4 are plotted the maximum transconductance (g_m) and transition frequency f_T as a function of the EOT. Thanks to improved electrostatic control through higher gate capacitance, reducing EOT always leads to a transconductance enhancement. The obtained results compare very well with a result of quantum NEGF simulation including electron–phonon scattering [24]. An experimental result [25] is also plotted. Given that possible parasitics are not included in the simulation the agreement can be considered as satisfactory.

It is remarkable that the transconductance improvement at low EOT is not fully reflected in the transition frequency $f_T = g_m/(2\pi C_{GS})$. Indeed, in quantum capacitance regime (EOT < 1 nm), the total gate capacitance increases more slowly than the transconductance when reducing EOT, which yields a small f_T decrease. It shows that the aggressive scaling of the gate oxide thickness is not useful to enhance the frequency performance of CNTFET, in contrast to the case of conventional Si MOSFET where the quantum capacitance regime is more difficult to reach. It should be noted that for a gate length of 300 nm a transition frequency of 205 GHz was obtained (not shown) which is much higher than the best experimental reported result of 30 GHz [26] for this non mature technology.

Fig. 5 compares typical I_D–V_{GS} characteristics obtained for ohmic and Schottky contact CNTFET with gate length of 100 nm. The equivalent oxide thickness of the cylindrical gate is 5 nm. The Schottky barrier height is $\Phi_{SB} =$

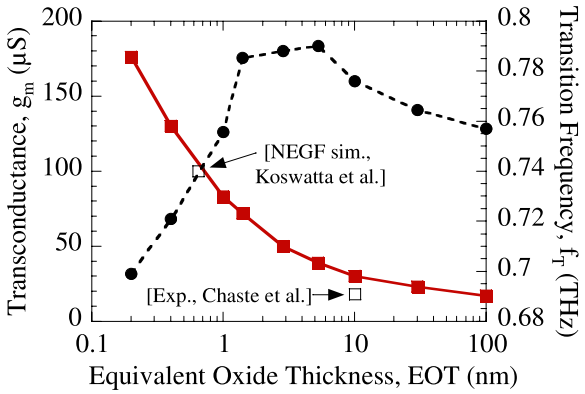

Fig. 4. Maximum transconductance (squares) and transition frequency (circles) of ohmic contact CNTFET as a function of equivalent oxide thickness ($L_G = 100$ nm, $V_{DS} = 0.4$ V). Transconductance is compared with a NEGF result including phonon scattering with $L_G = 30$ nm [24] and an experimental result for a single nanotube FET [25] (open square).

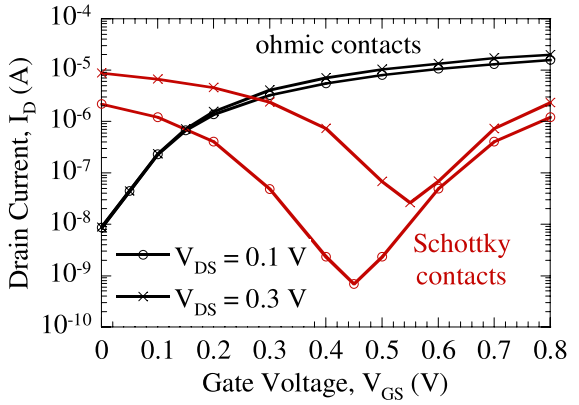

Fig. 5. Transfer characteristics of CNTFET with ohmic and Schottky source and drain contacts for $V_{DS} = 0.1$ V and $V_{DS} = 0.3$ V.

0.275 eV $= E_G/2$. The Schottky contact transistor is characterized by a strong ambipolar behaviour which degrades the subthreshold characteristics. For $V_{DS} = 0.3$ V the minimum subthreshold slope is about 95 mV/decade instead of 70 mV/decade in the ohmic contact device. As expected, the Schottky contacts are also detrimental to the on-state current. The transconductance is limited to 20.5 μS in the Schottky device instead of 32 μS in the ohmic one.

3.2. Comparison between compact model and Monte Carlo simulation

In this subsection, we briefly compare some results obtained from the compact model presented in Section 2 and the Monte Carlo simulation of transistors with ohmic source and drain contacts. The parameter values introduced into the compact model are as follows: Channel length, $L = 100$ nm, chirality and diameter, $(n, m) = (19, 0)$, Source/Drain resistance, $R_{S/D} \simeq 0$, Gate capacitance, Flat band voltage, $V_{FB} = -137.5$ mV, Fermi level in access S/D region, $E_F = 115$ meV, Electrostatic drain capacitance, $C_{DE} = 0.1$ aF, Electrostatic source capacitance, $C_{SE} = 0.7$ aF, Gate resistance, $R_G = 10\ \Omega$, Temperature, $T = 300$ K. According to the gate oxide thicknesses considered for the devices simulated by the Monte Carlo method, the values of insulator capacitances are $C_{INS} = 112, 225$ and 560 pF/m, respectively. Fig. 6 shows the results of source–drain current I_{DS} as a function of gate bias, for $V_{DS} = 400$ mV. A good agreement is found between compact modelling and Monte Carlo simulation. The detailed comparison of the results shows that in the present state the compact model is valid for bias conditions leading to flat potential in the access and the gated part of the channel, which ensures negligible effects of electron–phonon scattering [16].

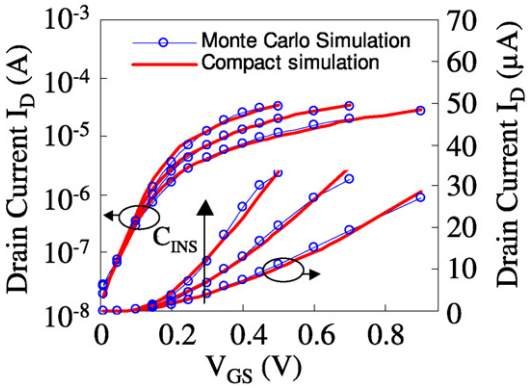

Fig. 6. Source–drain current, I_{DS} as a function of gate bias for $V_{DS} = 0.4$ V and for three gate capacitance values, $C_{INS} = 112, 225$ and 560 pF/m. Monte Carlo simulation (circles) and compact modelling (solid lines). The same data is shown in logarithmic scale (right) and linear scale (left).

4. Quantum device simulation

In order to describe accurately many aspects of electronic transport in nanodevices, it is necessary to take into account the quantum nature of electrons. Although quantum confinement of electronic states in the transverse directions is already included in the multiband effective mass models used in Sections 2 and 3, the wave nature of electrons along the transport direction can also have a strong impact on the device behaviour. There are several formalisms for studying quantum transport. The Wigner Monte Carlo method (WMC) allows a full quantum treatment of electron transport with the inclusion of phonon scattering, but it is limited to effective mass Hamiltonians. The Landauer–Büttiker (LB) and NEGF formalisms are useable with more general Hamiltonians. Of particular interest are tight-binding Hamiltonians, which describe electronic states at the atomic scale and can be derived from *ab initio* calculations, as will be shown is Section 5. This section is restricted to the simulation of ideal CNTFETs with simple Hamiltonians, using the WMC and NEGF methods.

4.1. Wigner Monte Carlo simulation

The quantum transport in nanodevices can be treated by making use of the Wigner's function (WF) that is defined in the phase space as a Fourier transform of the density operator [27,28]. In the classical limit this function reduces to the classical distribution function. The dynamical equation of the WF, i.e. the Wigner transport equation (WTE), is very similar to the BTE, except in the influence of the potential whose rapid space variations generate quantum effects. Again, in the classical limit of slow potential gradients the WTE reduces to the BTE. The strong analogy between Wigner and Boltzmann formalisms makes possible and appealing to adapt the standard MC technique to solve the BTE by just considering the WF as an ensemble of pseudo-particles [29]. Scattering effects may be easily included by using the same collision operator as in the BTE [28].

We recently developed a technique to solve the WTE for self-consistent simulation of RTDs [29]. It has been then applied to analyze the quantum transport effects in double-gate MOSFET for comparison with the semi-classical approximation [19], and to study the phonon-induced decoherence in nanodevices [30]. It is extended here to the case of coaxially-gated CNTFET, starting from a code initially developed for semi-classical simulation. In what follows semi-classical and quantum Monte Carlo simulation results are compared for a typical CNTFET with ohmic source and drain contacts. The device parameters used for the simulation are as follows: the gate length is 25 nm with a SiO_2 gate oxide thickness of 5.3 nm, the source and drain access are 20 nm-long with an N+ doping of 0.34 nm^{-1} and ohmic contacts. A semiconducting zigzag nanotube $(19, 0)$ is considered with a bandgap of 0.55 eV. The two first subbands are taken into account with effective masses of $0.048m_0$ and $0.129m_0$, respectively.

We first consider the on-state of the transistor, i.e. at $V_{GS} = V_{DS} = 0.4$ V. In Fig. 7 we plot the cartography in the phase space of the Boltzmann function f_b (from semiclassical calculation) and the Wigner function f_w (from quantum calculation). The two functions look very different. In the semi-classical case, the carriers are abruptly accelerated by the electric field at the drain-end of the channel. In contrast, in the quantum case, the acceleration seems much slower

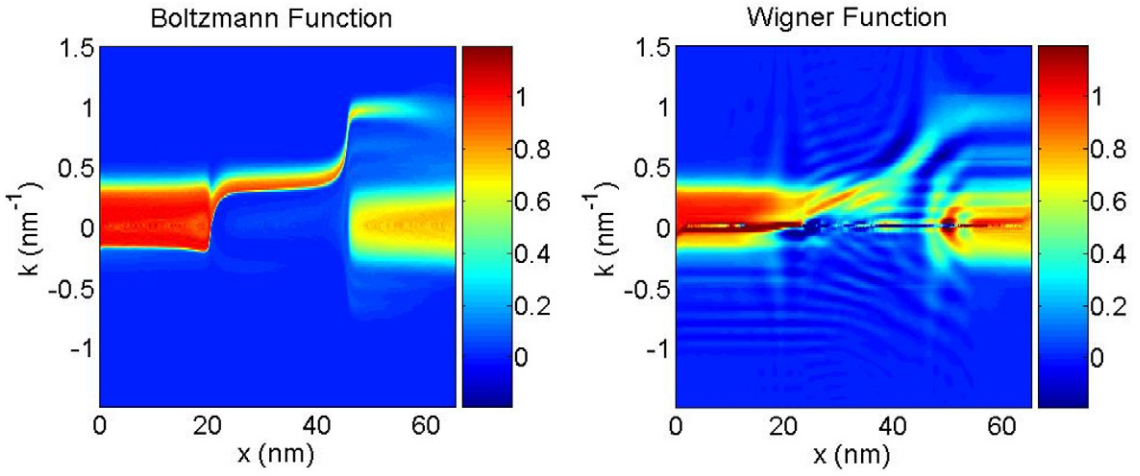

Fig. 7. Cartography of Boltzmann and Wigner functions from semi-classical and Wigner MC simulation of CNFET, respectively, for $V_{GS} = V_{DS} = 0.4$ V. The gate is located from $x = 20$ to 45 nm. k is the wavevector along the nanotube axis.

as if the carriers feel the potential fall in advance, which is consistent with the idea of delocalized electrons with finite extension of their wave function. Moreover, the positive–negative oscillations of the Wigner function at the drain-end of the gate are the signature of a strongly coherent transport. The quantum coherence between incident and reflected electrons also appears in the fast oscillations about $k = 0$.

In spite of these strong differences observed at microscopic level, it is noticeable to see that the two types of simulation give quite close terminal currents (not shown). In ON-state a drain current of 8.98 A is reached with semi-classical simulation while a value of 7.8 A is obtained in the quantum case. This difference is significant, but quite weak when one considers the microscopic pictures of Fig. 7. The difference is essentially due to quantum reflections occurring at the drain-end of the channel. It shows that microscopic quantum effects are not systematically strongly reflected at the macroscopic level of current. This result suggests that, at first order and without considering about atomistic effects, the semi-classical approach of transport may be acceptable much beyond its theoretical domain of validity.

4.2. NEGF simulation of nanotube transistors

The LB approach [31,32] is well suited for studying intrinsic transport in one dimensional systems such as nanotubes or nanowires. The low bias conductance is related to the transmission coefficient of electronic waves through the system connected to electrodes. Throughout this article, the energy-dependent conductance (also called "transmission") is given in G_0 units, where $G_0 = 2e^2/h$ is the quantum of conductance. The NEGF formalism [33,34] is an extension of the LB approach which allows one to treat a bias voltage applied between electrodes and to include some types of interactions inside the channel. It is widely used for the quantum simulation of nanodevices [35–37].

We have developed a NEGF code which can handle any type of tight-binding Hamiltonian. The Green's functions are computed using decimation and recursion algorithms [38,39]. They give the local charge density on each atom of the channel, and the LB electronic transmission. The charge density is coupled to a Poisson solver in order to obtain the self-consistent electrostatic potential in the presence of source, drain, and gate electrodes.

Here we present the simulation of a Schottky barrier CNTFET, in which the current is controlled by the tunneling through the barriers at the metal/nanotube contacts. A semiconducting nanotube with helicity $(10, 0)$ and a length of 30 nm is considered. It is described by a simple tight-binding Hamiltonian with one orbital per carbon atom and a nearest neighbour hopping energy $\gamma = 2.7$ eV. The all-around gate is 1.5 nm away from the nanotube surface. The model used here for electrodes is very simple: at both ends of the nanotube, carbon atoms are connected, via a hopping energy $\Delta = 1$ eV, to a fictive metal atom bearing a semi-elliptic density of states. The Fermi level of each electrode is aligned with the midgap of the nanotube, which gives a Schottky barrier $\Phi_{BS} = 0.45$ eV for both electrons and holes, and an ambipolar transistor behaviour. The electrons distribution in each electrode follows the Fermi–Dirac function at room temperature $T = 300$ K.

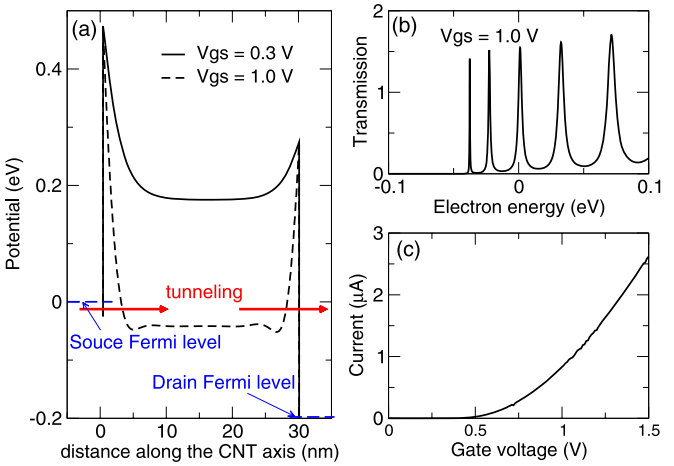

Fig. 8. Simulation of a Schottky barrier CNTFET using the NEGF technique. The source–drain voltage V_{DS} is set to 0.2 V. (a) Conduction band diagrams for two values of the gate voltage V_{GS}. The Schottky barriers widths decrease as V_{GS} increases. Once the width is small enough (a few nm), electrons can tunnel through the barriers. (b) Transmission spectrum at $V_{GS} = 1$ V, for energies around the source Fermi level. The peaks are due to the discrete energy levels in the quantum well formed in the channel between the two barriers. (c) Source–drain current versus gate voltage.

The obtained self-consistent potential profiles, electronic transmission, and source–drain current, are shown in Fig. 8. Only the n-type current is shown, since the p-type current is exactly symmetric in this case. The same type of calculation was already done by other authors [40]. Work is in progress in order to improve the contact models, using the *ab initio* results presented in Section 5.3. We also plan to use the tunneling transmission obtained with NEGF for validating or improving the Monte Carlo simulations of the Schottky barrier CNTFET presented in Section 3.

5. *Ab initio* calculations and their bridging to transport calculations in large systems

The *ab initio* calculations presented in this section are based on the density functional theory (DFT) and are performed with the Siesta package [41], which expresses the self-consistent Hamiltonian on a localized atomic orbital basis. The sparcity of the Hamiltonian is then exploited in a standard way to compute the Green's functions and the Landauer–Buttiker transmission of a system connected to semi-infinite periodic electrodes. The "Tablier" code, developed for this purpose, has been tested and used to study the conductance of doped nanotubes [42–44], graphene nanoribbons [45] and nanowires [46–48]. The Green's function technique used here is similar to those presented in Section 4.2 for simple tight-binding models, but Hamiltonians are much more realistic, with proper self-consistent charge transfers and hybridizations, and several orbitals per atom.

5.1. *Doped nanotubes: from ab initio to mesoscopic semi-empirical calculations*

The effect of a single impurity (boron, nitrogen, potassium, etc.) on the electronic and transport properties of nanotubes can be easily investigated using *ab initio* calculations. Besides the study now standard of the drop of conductance associated with a single impurity, the evolution of the self-consistent *ab initio* on-site and hopping matrix elements for the p_z orbitals (perpendicular to the tube wall) has been extracted to build a simplified scattering potential around the impurity (see Fig. 3 in Ref. [42]). By performing a transport calculation for the same geometry (isolated dopant) with a simplified $\pi - \pi^*$ tight-binding Hamiltonian, we verify that such a scattering potential allows to reproduce nicely the drop of conductance associated with the physics of resonant backscattering [49] at the energies of the bound states around the impurity (see insert of Fig. 9). The use of such an accurate $\pi - \pi^*$ tight-binding scattering potential around one dopant allows one further to perform calculations on micrometer long tubes with random doping, that is to bridge the gap with mesoscopic physics. By studying the conductance as a function of tube length and for several realizations of disorder, typical length scales such as the mean free path and localization length can be extracted and the Thouless relations relating these length scales can be verified for realistic potentials. Such

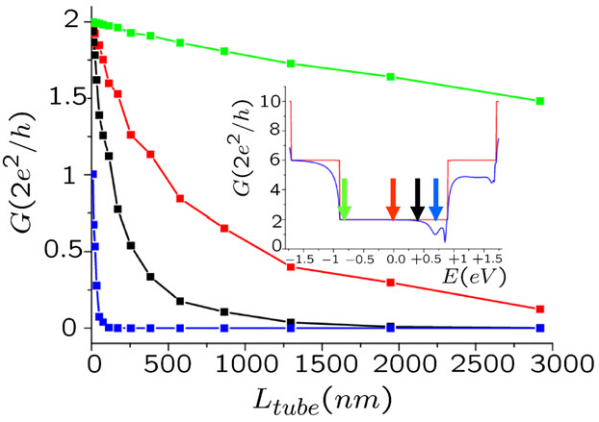

Fig. 9. Main frame: Length dependence of the Landauer conductance for the disordered (10, 10) nitrogen-doped nanotube at several energies (doping is fixed to 0.1%). Insert: Conductance versus energy for the perfect (dashed line) and single-impurity (solid line) cases. Arrows show the considered energies for the scaling analysis (main frame).

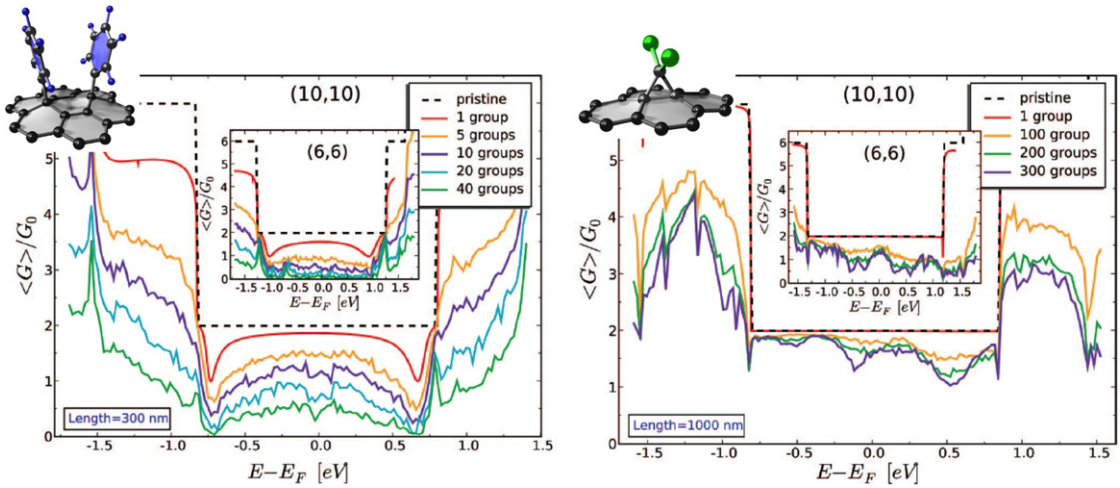

Fig. 10. Left: conductance of a (10, 10) metallic nanotube of length 300 nm with 1 to 40 bi-phenyl groups grafted at random locations (insert: (6, 6) nanotube). Right: same calculation for a 1 micrometer long nanotube with 1 to 300 carbene groups.

an analysis was performed in the case of Nitrogen-doped tubes [43,44] (see Fig. 9). The same approach is further expected to improve the impurity scattering description in device simulations (NEGF and Monte Carlo).

5.2. *Mesoscopic transport with ab initio calculations: the case of functionalized tubes*

While the building of a simple $\pi - \pi^*$ scattering potential is extremely reliable in the case of boron/nitrogen doping which preserves the decoupling with σ- and π-bonds, this is not the case when covalent doping by e.g. phenyl [50,51] or carbene groups [52] transforms sp^2 carbon sites into sp^3 four-fold coordinated atoms. In that case, it is necessary to adopt a larger basis accounting for the entire $n = 2$ (s, p_x, p_y, p_z) shell. The cost of performing full *ab initio* calculations with the double-zeta basis (8 orbitals) is still significantly larger than working with a simplified tight-binding (s, p_x, p_y, p_z) 4-orbital basis, but the difference is much reduced as compared to the simplified one-orbital per site $\pi - \pi^*$ model. Following several groups in the field [50,52–55] we performed fully *ab initio* mesoscopic physics analysis of micrometer long tubes functionalized with random coverage of covalently grafted moieties such as carbene and phenyl radicals [56]. The main outcome of our calculations (see Fig. 10) is that while covalent grafting of a few dozens of phenyl groups dramatically destroys the conductance of nanotubes, the grafting of several hundreds

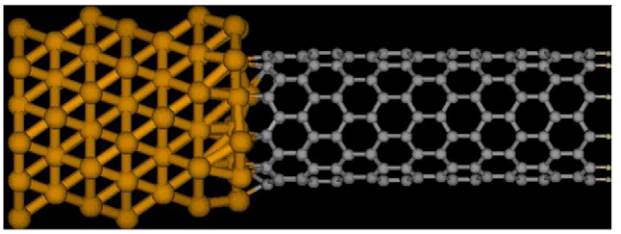

Fig. 11. Example of Pd/nanotube interface used in the Siesta calculation. It corresponds to a Pd nanowire with a "ABC" stacking connected to a $(10, 0)$ carbon nanotube with an end contact.

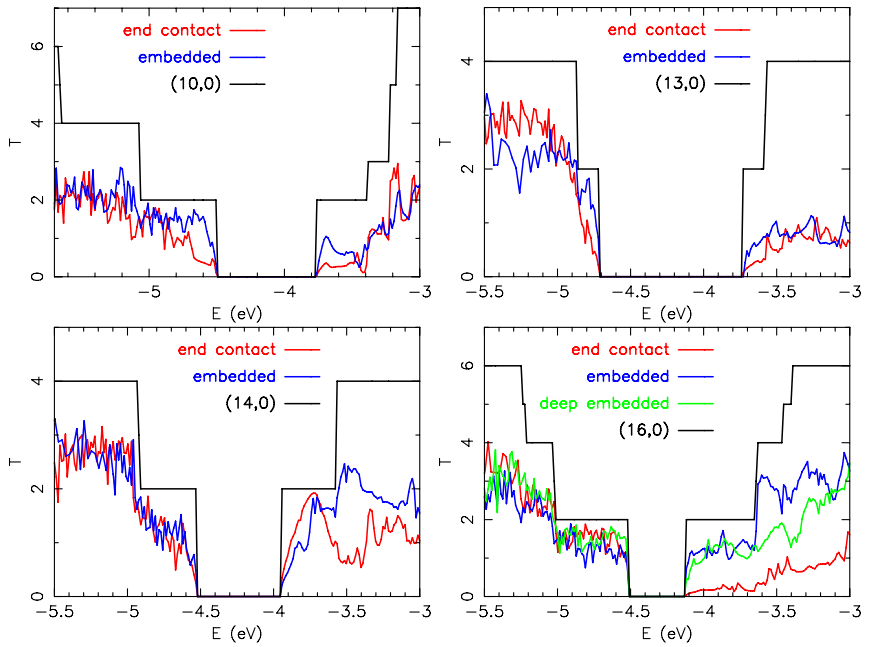

Fig. 12. Transmissions through the interface between a Pd nanowire and various semiconducting CNT. For each CNT, we have investigated two kinds of contact geometries: flat or embedded (for the $(16, 0)$ we present also a contact named "deep embedded" where 3 periods of the CNT are embedded). On each plot is given the transmission for the corresponding infinite CNT.

of carbene preserves more than 75% of the conductance at all energies on the main conduction $2G_0$ plateau in the case of metallic tubes.

5.3. Ab initio study of metal/nanotube contacts

Experimentally, it is observed that the nature of metal/CNT contacts strongly influences the CNTFET characteristics [3,4]. Moreover, the Schottky or ohmic character depends on the CNT diameter: for large diameter nanotubes (above 2 nm) with Palladium contacts, ohmic transport for holes is usually observed [57].

To investigate these issues, we have studied the influence of the CNT diameter and contact geometry. We restrict to Palladium contacts, considering the experimental observations [5,57] on this particular interface. The system used for this study is a Pd nanowire (with diameter from 0.85 nm to 1.30 nm) connected to $(n, 0)$ semiconducting carbon nanotubes, ranging from the $(7, 0)$ to the $(16, 0)$. All the structures are fully relaxed, using the Siesta package, with a force tolerance of 0.1 eV/Å. For each CNT we have investigated the influence of the contact geometry, considering an end contact where the CNT is contacted to a flat metal surface (Fig. 11), and an embedded one where one unit cell of the CNT is melted in the metal.

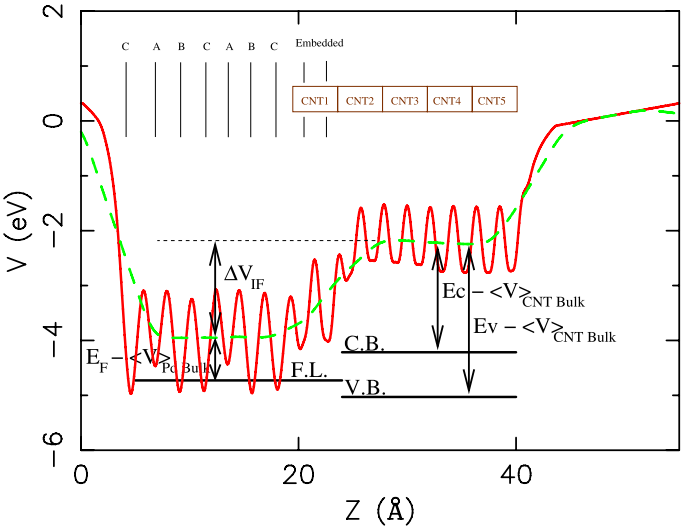

Fig. 13. Schematic representation of the average potential across the Pd/CNT interface, used to compute the Schottky barrier height. The solid line is the average potential along the xy plane. The dashed line is the same potential averaged along the z plane on one period of the metal and the CNT. ΔV_{IF} is the difference between the average potentials on the metal side and on the CNT side. The position, with respect to the average potentials, of the Fermi level of the metal (F.L.), of the conduction band (C.B.), and of the valence band (V.B.), are obtained from bulk calculations on Pd nanowire and CNT. The Schottky barrier height is obtained as (C.B. − F.L.) for electrons and (F.L. − V.B.) for holes.

The transmissions for various Pd-CNT interfaces are represented in Fig. 12. The relevant energy regions are the π and π^* bands, on both sides of the bandgap. Our results do not allow to conclude on a better quality of end or embedded contact. However, the π band transmission (p-type) is always larger than the π^* one (n-type), in agreement with previous calculations [58].

The second point investigated here is the Schottky barrier height (SBH) at the metal/CNT interface. The variation of the effective potential across the junction can be divided into a short range variation ($1 \simeq 2$ nm) and a long range variation associated with the space charge region. *Ab initio* calculations are restricted to the interface region, where a dipole between the metal and the semiconducting nanotube develops, due to metal induced gap states (MIGS) [59]. We focus here on the SBH for holes, defined as the difference between the Fermi level of the metal and the top of the valence band of the semiconductor. Since we are dealing with a finite size system, it is not easy to define these energy levels. To overcome this problem, *ab initio* calculations on bulk materials are combined with the results for the interface, as described by Duke et al. [60]. Fig. 13 illustrates how the average potential is combined to the bulk potentials to get the band alignment between the two materials. Two contributions to the SBH can be defined. The bare Mott–Schottky barrier is the difference between the Fermi level and the valence band maximum of the separate materials. It is obtained from bulk calculations, taking into account the work functions difference. The second contribution is due to the MIGS dipole.

Our calculations show that the MIGS contribution to the SBH is small, in agreement with the simple model of Ref. [61]. For the $(7, 0)$, the Mott–Schottky p-type SBH equals 0.11 eV, and the MIGS correction increases the SBH by 0.13 eV (embedded contact) or 0.11 eV (end contact). For the $(13, 0)$, the total SBH is -0.28 eV (p-type ohmic contact), with a MIGS correction of 0.06 eV. For all other helicities, the MIGS correction remains of the order of 0.1 eV. Thus the main contribution to SBH is the bare Mott–Schottky barrier, governed by the intrinsic properties of the bulk materials, i.e. band gap and electronic affinity. Moreover, the p-type SBH tends to be below the valence band for nanotube larger than the $(13, 0)$ which would lead to a p-type ohmic contact. This result is in qualitative agreement with the diameter dependence observed experimentally [57].

Work is in progress to combine these results with the NEGF device simulations presented in Section 4.2.

6. Conclusion

The simulation techniques presented in this article extend from the molecular scale to the circuit scale. Some links between the different techniques are established, such as the validation and improvement of compact models

by Monte Carlo device simulations, or the bridging between first principles calculation and quantum transport in nanotubes of realistic size. Work is in progress to develop the missing links between quantum transport approaches, Monte Carlo device simulations and compact modelling. One of the originality of our contribution lies in the cross-fertilization achieved by different communities of computational modelling and quantum simulation, which allows more standard simulation tools of microelectronics to be enriched by state of the art *ab initio* calculations. This opens new perspectives to assess the true potential of such BEYOND-CMOS devices either to compete against conventional silicon-based MOSFETs, or for providing innovative device functionalities.

Acknowledgements

We acknowledge support from the French National Research Agency, through the ANR/PNANO project ACCENT. A part of this work was supported by the European Community, through Network of Excellence NANOSIL (ICT-216171). We thank the CEA/CCRT supercomputing facilities for providing computational resources and technical support.

References

[1] J.C. Charlier, X. Blase, S. Roche, Electronic and transport properties of carbon nanotubes, Rev. Mod. Phys. 79 (2007) 677.
[2] S.J. Tans, M.H. Devoret, R.J.A. Groeneveld, C. Dekker, Room-temperature transistor based on a single carbon nanotube, Nature 393 (1998) 49.
[3] S. Heinze, J. Tersoff, R. Martel, V. Derycke, J. Appenzeller, Ph. Avouris, Carbon nanotubes as Schottky barrier transistors, Phys. Rev. Lett. 89 (2002) 106801.
[4] J. Appenzeller, J. Knoch, V. Derycke, R. Martel, S. Wind, Ph. Avouris, Field-modulated carrier transport in carbon nanotube transistors, Phys. Rev. Lett. 89 (2002) 126801.
[5] A. Javey, J. Guo, Q. Wang, M. Lundstrom, H. Dai, Ballistic carbon nanotube field-effect transistors, Nature 424 (2003) 654.
[6] S. Auvray, et al., Carbon nanotube chemistry and assembly for electronic devices, C. R. Physique, in this issue.
[7] S.M. Bachilo, L. Balzano, J.E. Herrera, F. Pompeo, D.E. Resasco, R.B. Weisman, Narrow (n, m)-distribution of single walled carbon nanotubes grown using a solid supported catalyst, J. Am. Chem. Soc. 125 (2003) 11186–11187.
[8] G.H. Jeong, A. Yamazaki, S. Susuki, H. Yoshimura, Y. Kobayashi, Y. Homma, Cobalt-filled apoferritin for suspended single-walled carbon nanotube growth with narrow diameter distribution, J. Am. Chem. Soc. 127 (2005) 8238–8239.
[9] M. Lee, J. Im, B.Y. Lee, S. Myung, J. Kang, L. Huang, Y.-K. Kwon, S. Hong, Linker-free directed assembly of high-performance integrated devices based on nanotubes and nanowires, Nature Nanotechnology 1 (2006) 66–71.
[10] M.S. Arnold, A.A. Green, J.F. Hulvat, S.I. Stupp, M.C. Hersam, Sorting carbon nanotubes by electronic structure using density differentiation, Nature Nanotechnology 1 (2006) 60–65.
[11] G.H. Jeong, A. Yamazaki, S. Suzuki, H. Yoshimura, Y. Kobayashi, Y. Homma, Production of single-walled carbon nanotubes with narrow diameter distribution using iron nanoparticles derived from DNA-binding proteins from starved cells, Carbon 45 (2007) 978–983.
[12] H. Hongo, F. Nihey, Y. Ochiai, Horizontally directional single-wall carbon nanotubes grown by chemical vapor deposition with a local electric field, J. Appl. Phys. 101 (2007) 024325.
[13] Y. Lu, S. Bangsaruntip, X. Wang, L. Zhang, Y. Nishi, H. Dai, DNA functionalization of carbon nanotubes for ultrathin atomic layer deposition of high K dielectrics for nanotube transistors with 60 mV/decade switching, J. Am. Chem. Soc. 128 (2006) 3518–3519.
[14] A. Raychowdhury, S. Mukhopadhyay, K. Roy, A circuit-compatible model of ballistic carbon nanotube field-effect transistors, IEEE Trans. Computer-Aided Design of Integrated Circuits and Systems 23 (10) (2004) 1411–1420.
[15] C. Maneux, J. Goguet, S. Frégonèse, T. Zimmer, H. Cazin d'Honincthun, S. Galdin-Retailleau, Analysis of CNTFET physical compact model, in: Proc. IEEE Int. Conf. Design & Test of Integrated Sys. (DTIS) in Nanoscale Technology, 2006, pp. 40–45.
[16] S. Frégonèse, H. Cazin d'Honincthun, J. Goguet, C. Maneux, T. Zimmer, J.P. Bourgoin, P. Dollfus, S. Galdin-Retailleau, Computationally efficient physics-based compact CNTFET model for circuit design, IEEE Trans. Electron Devices 55 (6) (2008) 1317–1327.
[17] C. Jacoboni, P. Lugli, The Monte Carlo Method for Semiconductor Device Simulation, Springer-Verlag, Wien–New York, 1989.
[18] C. Jungemann, B. Meinerzhagen, Hierarchical Device Simulation: The Monte Carlo Perspective, Springer, Wien–New York, 2003.
[19] D. Querlioz, J. Saint-Martin, K. Huet, A. Bournel, V. Aubry-Fortuna, C. Chassat, S. Galdin-Retailleau, P. Dollfus, On the ability of the particle Monte Carlo technique to include quantum effects in nano-MOSFET simulation, IEEE Trans. Electron Devices 54 (2007) 2232–2242.
[20] G. Pennington, N. Goldsman, Semi-classical transport and phonon scattering of electrons in semiconducting carbon nanotubes, Phys. Rev. B 68 (2003) 045426.
[21] H. Cazin d'Honincthun, S. Galdin-Retailleau, J. Sée, P. Dollfus, Electron–phonon scattering and ballistic behaviour in semiconducting carbon nanotubes, Appl. Phys. Lett. 87 (2005) 172112.
[22] A. Verma, et al., Effects of radial breathing mode phonons on charge transport in semiconducting zigzag carbon nanotubes, Appl. Phys. Lett. 87 (2005) 123101;
M. Machon, et al., Strength of radial breathing mode in single-walled carbon nanotubes, Phys. Rev. B 71 (2005) 035416.
[23] H. Nha Nguyen, H. Cazin d'Honincthun, C. Chapus, A. Bournel, S. Galdin-Retailleau, P. Dollfus, N. Locatelli, Monte Carlo modeling of Schottky contacts on semiconducting carbon nanotubes, in: Proc. SISPAD 2007, Vienna, Austria, Springer, 2007, pp. 313–316.

[24] S.O. Koswatta, S.H. Hasan, M.S. Lundstrom, M.P. Anantram, D.E. Nikonov, IEEE Trans. Electron Devices 54 (2007) 2339–2351.
[25] J. Chaste, L. Lechner, P. Morfin, G. Fève, T. Kontos, J.-M. Berroir, D.C. Glattli, H. Happy, P. Hakonen, B. Plaçais, Single carbon nanotube transistor at GHz frequency, Nano Lett. 8 (2008) 525–528.
[26] A. Le Louarn, F. Kapche, J.-M. Bethoux, H. Happy, G. Dambrine, V. Derycke, P. Chenevier, N. Izard, M.F. Goffman, J.-P. Bourgoin, Intrinsic current gain cutoff frequency of 30 GHz with carbone nanotube transistors, Appl. Phys. Lett. 90 (2007) 233108.
[27] C. Jacoboni, R. Brunetti, P. Bordone, A. Bertoni, Quantum transport and its simulation with the Wigner-function approach, Int. J. High Speed Electronics and Systems 11 (2001) 387–423.
[28] M. Nedjalkov, H. Kosina, S. Selberherr, C. Ringhofer, D.K. Ferry, Unified particle approach to Wigner–Boltzmann transport in small semiconductor devices, Phys. Rev. B 70 (2004) 115319.
[29] D. Querlioz, P. Dollfus, V. Nam Do, A. Bournel, V. Lien Nguyen, An improved Wigner Monte-Carlo technique for the self-consistent simulation of RTDs, J. Comput. Electronics 5 (2006) 443–446.
[30] D. Querlioz, J. Saint-Martin, A. Bournel, P. Dollfus, Wigner Monte Carlo simulation of phonon-induced electron decoherence in semiconductor nanodevices, Phys. Rev. B 78 (2008) 165306.
[31] R. Landauer, Spatial variation of currents and fields due to localized scatterers in metallic conduction, IBM J. Research and Development 1 (1957) 223.
[32] M. Büttiker, et al., Generalized many-channel conductance formula with application to small rings, Phys. Rev. B 31 (1985) 6207.
[33] C. Caroli, et al., Direct calculation of the tunneling current, J. Phys. C 4 (1971) 916.
[34] Y. Meir, N.S. Wingreen, Landauer formula for the current in an interacting electron region, Phys. Rev. Lett. 68 (1992) 2512.
[35] R. Lake, et al., Single and multiband modeling of quantum electron transport through layered semiconductor devices, J. Appl. Phys. 81 (1997) 7845.
[36] S. Datta, Electronic Transport in Mesoscopic Systems, Cambridge University Press, Cambridge, United Kingdom, 1995.
[37] S. Datta, Quantum Transport: Atom to Transistor, Cambridge University Press, Cambridge, United Kingdom, 2005.
[38] M.P. López Sancho, J.M. López Sancho, J. Rubio, Quick iterative scheme for the calculation of transfer matrices: application to Mo(100), J. Phys. F: Met. Phys. 14 (1984) 1205.
[39] G. Grosso, S. Moroni, G. Pastori Parravicini, Electronic structure of the InAs–GaSb superlattice studied by the renormalization method, Phys. Rev. B 40 (1989) 12328.
[40] J. Guo, S. Datta, M. Lundstrom, A numerical study of scaling issues for Schottky-barrier carbon nanotube transistors, IEEE Trans. Electron Devices 51 (2004) 172.
[41] D. Sanchez-Portal, P. Ordejon, E. Artacho, J.M. Soler, Density-functional method for very large systems with LCAO basis sets, Int. J. Quantum Chem. 65 (1997) 453–461.
[42] Ch. Adessi, S. Roche, X. Blase, Reduced backscattering in potassium-doped nanotubes:ab initio and semiempirical simulations, Phys. Rev. B 73 (2006) 125414.
[43] R. Avriller, S. Latil, F. Triozon, X. Blase, S. Roche, Chemical disorder strength in carbon nanotubes: Magnetic tuning of quantum transport regimes, Phys. Rev. B 74 (2006) 121406(R).
[44] R. Avriller, S. Roche, F. Triozon, X. Blase, S. Latil, Low dimensional quantum transport properties of chemically disordered carbon nanotubes: from weak to strong localization regimes, Mod. Phys. Lett. B 21 (2007) 1955.
[45] B. Biel, X. Blase, F. Triozon, S. Roche, Doping effects on charge transport in graphene nanoribbons, Phys. Rev. Lett. 102 (2009) 096803.
[46] M.V. Fernández-Serra, Ch. Adessi, X. Blase, Surface segregation and backscattering in doped silicon nanowires, Phys. Rev. Lett. 96 (2006) 166805.
[47] M.V. Fernández-Serra, Ch. Adessi, X. Blase, Conductance, surface traps and passivation in doped silicon nanowires, Nano Lett. 6 (2006) 2674–2678.
[48] X. Blase, M.V. Fernández-Serra, Preserved conductance in covalently functionalized silicon nanowires, Phys. Rev. Lett. 100 (2008) 046802.
[49] H.J. Choi, et al., Defects, quasibound states, and quantum conductance in metallic carbon nanotubes, Phys. Rev. Lett. 84 (2000) 2917.
[50] Y.-S. Lee, M.B. Nardelli, N. Marzari, Band structure and quantum conductance of nanostructures from maximally localized Wannier functions: the case of functionalized carbon nanotubes, Phys. Rev. Lett. 95 (2005) 076804.
[51] E.R. Margine, M.-L. Bocquet, X. Blase, Thermal stability of graphene and nanotubes covalent functionalization, Nano Lett. 8 (2008) 3315.
[52] Y.-S. Lee, N. Marzari, Cycloaddition functionalizations to preserve or control the conductance of carbon nanotubes, Phys. Rev. Lett. 97 (2006) 116801.
[53] C. Gómez-Navarro, et al., Tuning the conductance of single-walled carbon nanotubes by ion irradiation in the Anderson localization regime, Nature Mater. 4 (2005) 534.
[54] A.R. Rocha, et al., Designing real nanotube-based gas sensors, Phys. Rev. Lett. 100 (2008) 176803.
[55] T. Markussen, et al., Scaling theory put into practice: first-principles modeling of transport in doped silicon nanowires, Phys. Rev. Lett. 99 (2007) 076803.
[56] A. López-Bezanilla, F. Triozon, S. Latil, X. Blase, S. Roche, Effect of the chemical functionalization on charge transport in carbon nanotubes at the mesoscopic scale, Nano Lett. 9 (2009) 940.
[57] W. Kim, A. Javey, R. Tu, J. Cao, Q. Wang, H. Dai, Electrical contact to carbon nanotubes down to 1 nm in diameter, Appl. Phys. Lett. 87 (2005) 173101;
Z. Chen, et al., The role of metal-nanotube contact in the performance of carbon nanotube field-effect transistors, Nano Lett. 5 (2005) 1497.
[58] J.J. Palacios, P. Tarakeshwar, D.M. Kim, Metal contacts in carbon nanotube field-effect transistors: beyond the schottky paradigm, Phys. Rev. B 77 (2008) 113403.
[59] K. Odbadrakh, P. Pomorski, C. Roland, Ab initio band bending, metal-induced gap states, and schottky barriers of a carbon and a boron nitride nanotube device, Phys. Rev. B 73 (2006) 233402.

[60] R.G. Dandrea, C.B. Duke, Calculation of the Schottky barrier height at the Al/GaAs(001) heterojunction: Effect of interfacial atomic relaxations, J. Vac. Sci. Technol. A 11 (1993) 848–853.
[61] F. Léonard, J. Tersoff, Role of Fermi-level pinning in nanotube Schottky diodes, Phys. Rev. Lett. 84 (2000) 4693–4696.